Bottom-up approach for microstructure optimization of sound absorbing materials

Camille Perrot,[a] Fabien Chevillotte, and Raymond Panneton
Groupe d'Acoustique de l'Université de Sherbrooke (GAUS), Department of Mechanical Engineering, Université de Sherbrooke, Quebec J1K 2R1, Canada

(Received 8 January 2008; revised 8 May 2008; accepted 15 May 2008)

Results from a numerical study examining micro-/macrorelations linking local geometry parameters to sound absorption properties are presented. For a hexagonal structure of solid fibers, the porosity ϕ, the thermal characteristic length Λ', the static viscous permeability k_0, the tortuosity α_∞, the viscous characteristic length Λ, and the sound absorption coefficient are computed. Numerical solutions of the steady Stokes and electrical equations are employed to provide k_0, α_∞, and Λ. Hybrid estimates based on direct numerical evaluation of ϕ, Λ', k_0, α_∞, Λ, and the analytical model derived by Johnson, Allard, and Champoux are used to relate varying (i) throat size, (ii) pore size, and (iii) fibers' cross-section shapes to the sound absorption spectrum. The result of this paper tends to demonstrate the important effect of throat size in the sound absorption level, cell size in the sound absorption frequency selectivity, and fibers' cross-section shape in the porous material weight reduction. In a hexagonal porous structure with solid fibers, the sound absorption level will tend to be maximized with a 48 ± 10 μm throat size corresponding to an intermediate resistivity, a 13 ± 8 μm fiber radius associated with relatively small interfiber distances, and convex triangular cross-section shape fibers allowing weight reduction.
 [DOI: 10.1121/1.2945115]

PACS number(s): 43.50.Gf, 43.20.Hq, 43.20.Wd, 43.20.El [KA] Pages: 940–948

I. INTRODUCTION

A major issue in automobile, aeronautical, and building industries concerns the need to increase or adapt the sound absorption spectrum of commonly used sound absorbing materials. However, the most advanced models used to characterize and predict sound absorbing material performances are mainly based on interdependent macroscopic parameters, which do not take explicitly into account the local geometry of the porous media (i.e., its microstructure). For these reasons, optimizing sound absorbing materials from their fabrication remains a difficult task mostly done by trial and error. A strict optimization method would firstly rely on our ability to predict the acoustic properties of porous media from the description of their local geometry. Secondly, it would propose pertinent realistic modifications of their microstructure having predictable impacts on their absorption spectrum. The intent of this paper is to present such an optimization procedure following the bottom-up approach (i.e., from an optimized microstructure to the desired acoustical macroscopic behavior).

How do local geometry parameters relate to sound absorption spectrum in porous media? How do macroscopic flow and thermal properties depend on throat size, cell size, and fibers' cross-section shape? These are two of the many questions that dominate studies of relationships between microstructure and acoustic properties of porous media such as open-cell foams and fibrous materials. Such questions may be addressed in different manners. A common method consists in conducting a lot of laboratory measurements on samples of varying microstructural parameters.[1,2] Alternatively, in a search for a theoretical understanding, one may try to better understand the mathematical and physical basis of the macroscopic equations governing acoustic dissipation phenomena.[3–8] Also, numerical studies based on simulations can be considered.[9–16] Finally, recent studies include hybrid[17] approaches combining numerical predictions of key physical parameters used as input data in empirical models.[18] Each of these ways of considering these questions has advantages and disadvantages. Laboratory measurements are of indisputable value; however, their interpretation may be limited to a specific group of materials. Theoretical studies at the macroscopic scale lead to robust models, but they also require measurements of nonindependent macroscopic parameters. Numerical simulations usually attempt to bridge the gap between theory and experiments. They are nevertheless typically restrained by either the need to simplify geometry, physics, or both. Finally, hybrid approaches suffer from the weakness of empirical models providing poor physical insight and being unable to consider already nonexisting microstructural configurations.

In recent years, another approach to the numerical study of long-wavelength acoustic properties of porous media has gained some interests. The idea is to numerically solve, in a microstructural configuration that consists of a periodic unit cell (PUC), the linearized Navier–Stokes equation in harmonic regime with the local incompressibility condition[11] (dynamic viscous problem) and the linearized heat equation in harmonic regime[8] (dynamic thermal problem), with appropriate boundary conditions, and then to study how volume-averaged properties of the velocity and thermal fields relate

[a]Author to whom correspondence should be addressed. Electronic mail: camille.perrot@usherbrooke.ca

to microscopic details of the geometry. Compared to macroscopic models, such an approach offers the ability to study the microphysical basis of the acoustical macrobehavior.

For the case of the dynamic viscous problem, solutions mainly based on finite element methods (FEMs) have been investigated. Craggs and Hildebrandt[9] solved the viscous problem for specific cross sections of uniform pores. Wang and Lu[10] determined the optimized acoustic properties of polygonal ducts through semianalytical solutions. Zhou and Sheng[11] treated the case of a cylindrical tube with sinusoidal modulation of its cross section, and three-dimensional (3D) fused-spherical-bed and fused-diamond lattices. Firdaouss *et al.*[12] paid attention to a corrugated pore channel. Cortis *et al.*[13] studied the case of two-dimensional (2D) configurations made of a square arrangement of solid cylinders. They were also interested by the corrugated pore channel.[14] Gasser *et al.*[15] treated the 3D case of the face centered cubic sphere packing. An attempt to grasp the viscous dynamic behavior of more complex microstructures, such as a real open-cell aluminum foam sample, has also been carried out recently; thanks to a basic 2D model geometry with a relatively good success.[16]

Alternatively, the random-walker simulation method has been recently proposed by Lafarge[19] to provide an efficient resolution of the dynamic thermal problem. The principle of the method consists in simulating Brownian motion for a large number of the fluid-phase particles, and to link their mean square displacements to the thermal conduction properties of the confined fluid. An important point of the method is that, once the mean square displacements of a large number of particles have been estimated, the dynamic thermal response might be obtained for all frequencies. Contrary to finite element analysis, the solution has not been computed at each frequency. The random-walker simulation method has been implemented in two and three dimensions for computing the trapping constant of a 2D arrangement of overlapping fibers of circular cross sections,[20] and 3D digitalized geometries.[21] However, the trapping constant only provides the asymptotic low frequency behavior of the thermal problem. The first numerical simulations in harmonic regime have recently been proposed for the case of 2D regular and random arrangements of fibers with circular cross sections.[19] This work has been extended to 3D PUC, and applied to the determination of the dynamic thermal characteristics of an open-cell aluminum foam.[22,23]

Starting from these microphysical foundations, the aim of this paper is to illustrate the potential of such a bottom-up approach for microstructure optimization of highly porous open-cell foams and fibrous sound absorbing materials. In the framework of this paper, only the dynamic viscous boundary value problem is considered. The porous structure is a hexagonal lattice of solid fibers in air. For this simple geometry, it is shown how local geometry parameters are related to the sound absorption spectrum of the porous media through the main macroscopic parameters, giving a physical insight for why it was achieved. In particular, we will examine the influence of (i) the throat size, (ii) the cell size, and (iii) the cross-section shape of the fibers (i.e., circle, convex, straight, and concave triangles). An outline of this paper is as follows: In Sec. II, the model geometry and computational method behind the bottom-up approach are introduced. In Sec. III, results on a hexagonal structure of solid fibers are presented.

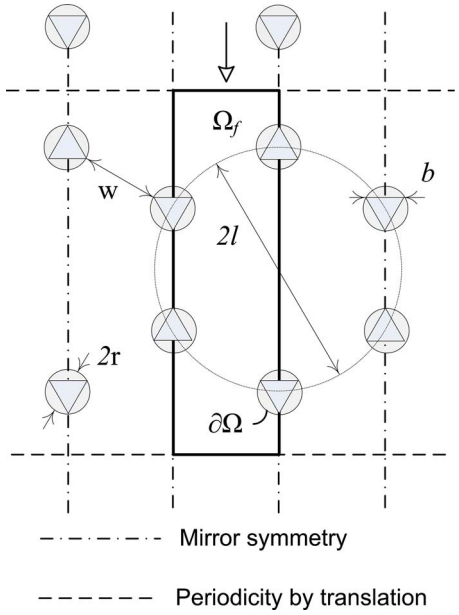

FIG. 1. (Color online) Local geometry model showing solid fibers having circular or triangular cross section shapes arranged in a hexagonal pattern. Triangular cross sections are considered to be inscribed in the corresponding circular ones. Numerical computations are performed at the scale of a vertical identified periodic unit cell (PUC).

II. NUMERICAL CALCULATIONS

A. Model geometry

A typical 2D hexagonal arrangement of fibers having l and r as local characteristic dimensions is depicted in Fig. 1. The fibers (the solid phase) are assumed motionless and diluted in air (the fluid phase). Their cross sections form the nodes of the hexagons. In this illustration, the cross sections of the fibers are circular. This is a typical case for a porosity $\phi \approx 0.85$ (or less). There are experimental evidences[24] that the cross-section shape of a foam ligament evolves from a circle ($\phi \approx 85\%$) for low porosity foams to convex ($\phi \approx 90\%$), straight ($\phi \approx 94\%$), and concave ($\phi \approx 98\%$) triangles for high porosity foams. For this reason, the shape of the cross section will be also considered as a local geometry parameter. See Fig. 2 for an illustration of the different cross-section shapes used in this study.

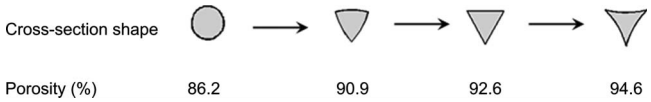

FIG. 2. Cross-section shapes and associated porosity values considered in this study. The porosity values are obtained with $r=32$ μm and $w=70$ μm. Triangular cross-section shapes (convex, straight, and concave) are inscribed in the initial circular cross section.

B. Computational method

The problem is addressed in three main steps: (1) solve numerically the asymptotic low (steady Stokes) and high (electric) frequency viscous boundary value problems using the FEM; (2) compute the static viscous permeability k_0, the viscous characteristic length Λ, and the tortuosity α_∞, as defined by Johnson *et al.*[4] by appropriate volume averaging of the corresponding asymptotic velocity fields; and (3) derive the frequency-dependent viscous and thermal response functions such as the effective density $\rho(\omega)$ and bulk modulus $K(\omega)$ of the entrained fluid in the rigid frame porous medium from the previously computed macroscopic parameters using the analytical models of Johnson *et al.*[4] and Allard and co-workers,[5,6] respectively, from which an approximate but robust description of propagation and absorption phenomena of an acoustic wave through a porous medium is entirely known.[6] Then, modification of the local geometry parameters by an iteration process allows us to maximize the area under the sound absorption coefficient curve in the frequency range of interest (here, from 10 to 10 000 Hz).

1. Asymptotic boundary value problems

At the zero angular frequency ($\omega=0$), the following set of equations is observed:

$$-\nabla\pi+\Delta\mathbf{w}+\mathbf{e}=0 \quad \text{in } \Omega_f, \tag{1}$$

$$\nabla\cdot\mathbf{w}=0 \quad \text{in } \Omega_f, \tag{2}$$

$$\mathbf{w}=0 \quad \text{on } \partial\Omega, \tag{3}$$

with the condition that π is a stationary field, simply describing the viscous fluid motion created in a porous medium in steady state regime. This is the steady Stokes problem in the fluid volume Ω_f for periodic structures (see Fig. 1), where $\mathbf{w}$ is the scaled static velocity field in the pore in m^2, and $\mathbf{e}$ is a unit vector. In what follows, the symbol $\langle\ \rangle$ designates a fluid-phase average. Writing the pressure p in terms of its mean and deviatoric parts, $p=\langle p\rangle+\Pi$ with $\langle\Pi\rangle=0$, the macroscopic pressure gradient is related to $\mathbf{e}$ in Eq. (1) by $\nabla\langle p\rangle=-|\nabla\langle p\rangle|\mathbf{e}$. The small fluctuation Π is related to π by $\Pi=|\nabla\langle p\rangle|\pi$. Finally, the static velocity field $\mathbf{v}$ is related to $\mathbf{w}$ by $\mathbf{v}=|\nabla\langle p\rangle/\eta|\mathbf{w}$, where η is the dynamic viscosity of the fluid.

At the opposite frequency range, when ω becomes very large, the viscous boundary layer becomes negligible and the fluid tends to behave as a perfect one, having no viscosity. In these conditions, the perfect incompressible fluid formally behaves according to the electric problem.[3] This electric problem is relevant to sound propagation as long as the wavelength is large enough for the saturating fluid to behave as an incompressible fluid in volumes of the order of the homogenization volume (a period in the case of periodic structure). $\mathbf{E}$ is the scaled electric field that solves the corresponding electrical conduction problem for a porous medium filled with a conducting fluid and having an insulating solid phase, i.e.,

$$\mathbf{E}=-\nabla\varphi+\mathbf{e} \quad \text{in } \Omega_f, \tag{4}$$

$$\nabla\cdot\mathbf{E}=0 \quad \text{in } \Omega_f, \tag{5}$$

$$\mathbf{E}\cdot\mathbf{n}=0 \quad \text{on } \partial\Omega, \tag{6}$$

and φ is a spatially stationary or periodic scalar field representing the deviatoric part of the electric potential.

The so-called steady Stokes and electric boundary value problems have been solved using a commercial finite element code[25] on the hexagonal 2D porous structure (cellular). No-slip boundary conditions at the pore walls, and periodicity of π were prescribed (then the static velocity field $\mathbf{w}$ is automatically periodic). For the electric problem, Neumann boundary conditions on the fluid-solid interface, and periodicity of φ on the inlet-outlet surfaces were used. Generalized Neumann boundary conditions are set in the remaining borders due to the symmetries of the problems. Calculations were performed with varying grid size to check the convergence of the results. Up to a total of 15 elements were used in the thickness of the viscous boundary layer. The symmetry property[26] of the viscous permeability tensor was also checked to guarantee the variation of the asymptotic solutions to less than a percent.

2. Macroscopic parameters' evaluation

Macroscopic parameters are then derived from the flow field solutions by spatial averaging. The open porosity ϕ was computed from the volume of the mesh, and the thermal characteristic length Λ' defined as the fluid-phase volume to wet surface ratio was obtained by the volume to wet surface ratio of the mesh. The static viscous permeability k_0 is computed from the static velocity field, and the viscous characteristic length Λ and the tortuosity α_∞ are computed from the electric field as defined by Johnson *et al.*[4] The components k_{0ij} defining the static viscous permeability tensor are simply given by[16]

$$k_{0ij}=\phi\langle\mathbf{w}^j\cdot\mathbf{e}^i\rangle, \tag{7}$$

where the superscript j refers to the direction of the imposed pressure gradient, and the components of $\mathbf{e}^i$ are $e^i_j=\delta_{ij}$ (with $\delta_{ij}=1$ if $i=j$ and $\delta_{ij}=0$ if $i\neq j$). In the studied configuration shown in Fig. 1, the gradient is along the vertical axis.

The components $\alpha_{\infty ij}$ defining the tortuosity tensor are derived from[27]

$$\alpha^{-1}_{\infty ij}=\langle\mathbf{E}^j\cdot\mathbf{e}^i\rangle, \tag{8}$$

where $\alpha^{-1}_{\infty ij}$ is the inverse of the tortuosity tensor $\alpha_{\infty ij}$. The viscous characteristic length Λ is computed using the definition of Johnson *et al.*[4] as follows:

$$2/\Lambda=\int_{\partial\Omega}\mathbf{E}^2dS/\int_{\Omega}\mathbf{E}^2dV, \tag{9}$$

who introduced this length-scale parameter Λ as the weighted pore volume to wet surface ratio. In the case of microscopic anisotropy for periodic porous structures such as the one studied here, static viscous permeability k_{0ij} and tortuosity $\alpha_{\infty ij}$ tensors reduce to scalars k_0 and α_∞, respectively.[26] This property makes implicitly reference to a

generalization in harmonic regime of the proof given by Torquato for the symmetry property in static regime in Ref. 26.

3. Analytical models

Equations derived by Johnson *et al.*[4] and Allard and co-workers[5,6] are then used to relate the macroscopic parameters to the effective density and bulk modulus of a fluid filled porous medium. The frequency-dependent absorption coefficient is then expressed from these quantities.[6] Note that the way the problem is addressed can eventually be refined by considering the computation of additional macroscopic parameters such as the static viscous tortuosity α_0, the static thermal permeability k_0', and the static thermal tortuosity α_0' defined by Lafarge *et al.*[8,27,28] as successive improvements of the modeled frequency-dependent viscous and thermal response functions.

Effective density and bulk modulus functions can be conveniently represented by the following approximate models:

$$\rho(\omega) = \rho_0 \alpha_\infty \left[1 + \frac{1}{i\varpi} f(\varpi) \right], \tag{10}$$

$$\frac{1}{K(\omega)} = \frac{1}{K_a} \left\{ \gamma - (\gamma - 1) \left[1 + \frac{1}{i\varpi'} f'(\varpi') \right]^{-1} \right\}, \tag{11}$$

where $K_a = \gamma P_0$ is the adiabatic bulk modulus, γ is the specific heat ratio, and P_0 the atmospheric pressure. ϖ and ϖ' are dimensionless viscous and thermal angular frequencies given by the following expressions:

$$\varpi = \frac{\omega}{\nu} \frac{k_0 \alpha_\infty}{\phi} \tag{12}$$

and

$$\varpi' = \frac{\omega}{\nu'} \frac{k_0'}{\phi}, \tag{13}$$

with $\nu = \eta/\rho_0$, $\nu' = \nu/\mathrm{Pr}$, Pr the Prandtl number, and the following shape functions f and f':

$$f(x) = 1 - P + P\sqrt{1 + \frac{M}{2P^2} ix}, \tag{14}$$

$$f'(x) = 1 - P' + P'\sqrt{1 + \frac{M'}{2P'^2} ix}, \tag{15}$$

where the dimensionless shape factors have been introduced:

$$M = \frac{8 k_0 \alpha_\infty}{\Lambda^2 \phi}, \tag{16}$$

$$M' = \frac{8 k_0'}{\Lambda'^2 \phi}, \tag{17}$$

$$P = \frac{M}{4\left(\frac{\alpha_0}{\alpha_\infty} - 1 \right)}, \tag{18}$$

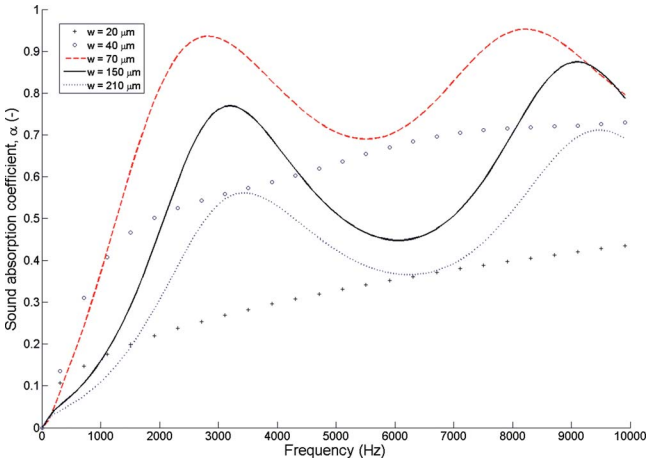

FIG. 3. (Color online) Effect of throat size w in the range 20–210 μm on the sound absorption coefficient. r is fixed at 200 μm.

$$P' = \frac{M'}{4(\alpha_0' - 1)}. \tag{19}$$

It can be seen that for $P = P' = M' = 1$, the model reduces to the so-called Johnson–Allard–Champoux model.

Although additional macroscopic parameters, as well as local geometry parameters can be considered, the focus of this analysis is practical trend exploration of sound absorption due to porous media morphology; how throat size, cell size, and cross-section shape of the ligaments influence sound absorption coefficient through the main macroscopic parameters in an idealized highly porous open-cell foam or fibrous absorber.

III. RESULTS AND DISCUSSION

A number of local geometry calculations are presented to illustrate the use of the computational method in maximizing the absorption coefficient of a hard backed 2D hexagonal porous structure having a total thickness of 25 mm for varying (i) throat sizes, (ii) cell sizes, and (iii) fiber cross-section shapes. To do so, the following sound absorption performance index will be used:

$$I = \frac{1}{N} \sum_{i=1}^{N} \alpha(\omega_i), \tag{20}$$

where $\alpha(\omega_i)$ is the normal incidence sound absorption computed at the ith angular frequency, and N is the number of discrete angular frequencies used in the frequency range of interest—here 10–10 000 Hz. For a given configuration, this indicator has to be maximized to yield the optimized local parameters.

A. Effect of throat size

Consider a plane acoustic wave propagating through the porous structure depicted in Fig. 1. The initial radius value of the circular cross-section fiber was fixed at $r \approx 200$ μm. Then, by an iteration process, the optimal throat size $w_{\mathrm{opt}} = 70$ μm was clearly determined, as shown in the plot of Fig. 3. For the initial r value, l was varied incrementally with a 10 μm step in the range 420–610 μm to find the optimum

TABLE I. Numerical evaluation of the main macroscopic parameters associated with a hexagonal porous structure of solid fibers with circular cross-section shapes for varying throat size values at constant fiber radius $r=200$ μm.

Throat size w (μm)	Porosity ϕ (%)	Thermal characteristic length Λ' (μm)	Viscous characteristic length Λ (μm)	Static airflow resistivity σ (N m^{-4} s)	Tortuosity α_∞ (−)	Performance index I (%)
20	45.16	165	37	1 108 618	2.05	30.47
30	47.68	182	54	408 035	1.77	46.12
40	50.03	200	71	201 463	1.61	58.17
50	52.23	219	87	116 813	1.50	66.46
60	54.28	237	103	74 965	1.43	71.50
70	56.21	257	119	51 591	1.37	73.68
80	58.01	276	135	37 365	1.33	73.58
90	59.71	296	150	28 136	1.30	71.94
100	61.31	317	166	21 845	1.27	69.40
110	62.81	338	181	17 386	1.25	66.41
120	64.22	359	196	14 123	1.23	63.29
130	65.56	381	211	11 670	1.22	60.21
140	66.83	403	226	9 784	1.20	57.26
150	68.02	425	241	8 306	1.19	54.49
160	69.15	448	256	7 129	1.18	51.91
170	70.23	472	271	6 177	1.17	49.53
180	71.24	496	286	5 398	1.16	47.32
190	72.21	520	301	4 752	1.15	45.29
200	73.13	544	316	4 213	1.14	43.40
210	74.00	569	332	3 757	1.14	41.65

$l=470$ μm, which yielded the maximum area under the absorption curve over the maximum possible area under the absorption curve, that is, $I_{opt}=73.67\%$. Note that at $l=480$ μm, similar global performances are obtained with $I=73.58\%$. The corresponding absorption spectrum is characterized by a higher absorption peak. More generally, for $460\ \mu\text{m}\leq l\leq 490\ \mu\text{m}$, that is, $60\ \mu\text{m}\leq w\leq 90\ \mu\text{m}$, the global absorption performances are systematically higher than $95\%\times I_{opt}\approx 70\%$, corresponding to an intermediate static airflow resistivity (defined as $\sigma=\eta/k_0$) range between 28 000 and 75 000 N m^{-4} s, see Table I.

B. Effect of fiber radius

Next, by setting $w=w_{opt}$, r was varied to find the optimum r_{opt}. r was initially varied with ten linearly spaced values in the range 50–350 μm. As index I decreases, a new iterative process was performed with ten linearly spaced values in the lower range 5–45 μm. The optimal fiber radius $r_{opt}=32$ μm was then determined with $I_{opt}=82.84\%$ and a static airflow resistivity equal to 26 758 N m^{-4} s, see Table II. Note that for a relatively large range of fiber radius, $10\ \mu\text{m}\leq r\leq 83\ \mu\text{m}$, $I\geq 95\%\times I_{opt}$, see Fig. 4. More generally, compared to the previous case, significant sound absorption enhancement can be obtained by keeping the optimal throat size and reducing the fiber radius, thus reducing in the mean time the cell sizes, which appear to be an argument in favor of small cell sizes ($2l=268$ μm) rather than the large ones ($2l=940$ μm). This phenomenon can be interpreted in terms of absorption frequency selectivity, where, given an optimal throat size and around the optimum fiber radius, a design choice could be made in terms of a rather large band or a relatively low frequency range absorption. Also interesting is the fact that the optimal fiber radius at constant throat size tends to minimize both viscous and thermal characteristic lengths, see Table II. This can be seen as a new criterion for pore (cell) size optimization at constant window (throat size) dimension.

C. Effect of cross-section shape

For the same geometry as considered in Fig. 1, the effect of the ligament cross-section shape on the sound absorption coefficient was also examined. Holding *a priori* w_{opt} and r_{opt} fixed, the cross-section shape c has to be searched to find the optimum c_{opt}. As previously mentioned in Sec. II A, the evolution of the fiber cross-section shape from a circle to a concave triangle is experimentally associated with an increasing porosity—see Fig. 2. With the aim to reflect this tendency, triangular cross sections were inscribed into the circular cross section, while keeping Λ' constant. However, this last condition, which is important to isolate the cross-section shape effect, also implies that the initial length between two ligaments associated with w_{opt} has to be modified. For the case of a straight triangular cross section, l can be expressed analytically as a function of Λ' in the following form: $l=\sqrt{(6b\Lambda'+\sqrt{3}b^2)/3\sqrt{3}}$, where $b=r_{opt}\sqrt{3}$. The next step is then to express l as a function of Λ' when considering the remaining cross-section shapes, convex and concave triangles. One more local geometry variable has to be taken into account, the convexity/concavity radius of curvature R, but it seems reasonable to state that $R\sim l$ from geometric considerations, see Fig. 1. Starting from macro-/microanalytical relationships linking Λ' to l, i.e.,

TABLE II. Numerical evaluation of the main macroscopic parameters associated with a hexagonal porous structure of solid fibers with circular cross-section shapes for varying fiber radius at constant throat size $w = 70\ \mu$m.

Fiber radius r (μm)	Porosity ϕ (%)	Thermal characteristic length Λ' (μm)	Viscous characteristic length Λ (μm)	Static airflow resistivity σ (N m^{-4} s)	Tortuosity σ_∞ (−)	Performance index I (%)
5	99.06	524	265	16 565	1.00	75.03
9	97.27	336	173	19 562	1.01	79.13
14	95.12	271	142	21 557	1.02	80.98
18	92.86	238	127	23 119	1.03	81.96
23	90.60	220	120	24 453	1.04	82.48
27	88.43	208	115	25 651	1.05	82.74
32	86.36	200	113	26 758	1.06	82.84
36	84.41	196	111	27 796	1.07	82.82
41	82.58	192	110	28 780	1.08	82.73
45	80.87	190	110	29 718	1.09	82.58
50	79.08	189	110	30 725	1.10	82.37
83	70.02	195	112	36 588	1.17	80.42
117	64.22	209	115	41 504	1.23	78.30
150	60.25	227	117	45 832	1.29	76.32
183	57.37	247	118	49 751	1.35	74.52
217	55.19	267	120	53 364	1.40	72.88
250	53.48	287	121	56 734	1.46	71.38
283	52.10	308	122	59 908	1.51	70.01
317	50.98	329	123	62 917	1.56	68.76
350	50.03	350	124	65 784	1.61	67.60

$$\Lambda' = \frac{l\sqrt{3}}{4\arcsin(b/2l)}\phi, \tag{21}$$

with

$$\phi = 1 - \left\{ \frac{b^2\sqrt{3}}{2} \pm 6\left[l^2 \arcsin\left(\frac{b}{2l}\right) - \frac{bl}{2}\sqrt{1-\frac{b^2}{4r^2}}\right]\right\} \Bigg/ \frac{3\sqrt{3}}{2}l^2, \tag{22}$$

a numerical inversion can be obtained after replacing $\arcsin(b/2l)$ and $\sqrt{1-b^2/4r^2}$ with their respective truncated Taylor expansions at order 3, $b/2l + b^3/48l^3$ and $1 - b^2/8l$. It finally yields $w_{opt} \approx 53\ \mu$m whatever the triangular cross-section shape.

As shown in Fig. 5 and Table III, the sound absorption performance index of a stack of fibers or open-cell foams with ligaments of convex, straight, and concave triangular cross-section shapes are slightly enhanced compared to those with a circular cross-section shape. More importantly, the porosity is actually significantly increasing with concavity, which is a compatible feature with foams' fabrication process.[24] Furthermore, the sound absorption enhancement with cross-section shape concavity is still associated with Λ minimization as it can be observed in Table III, which con-

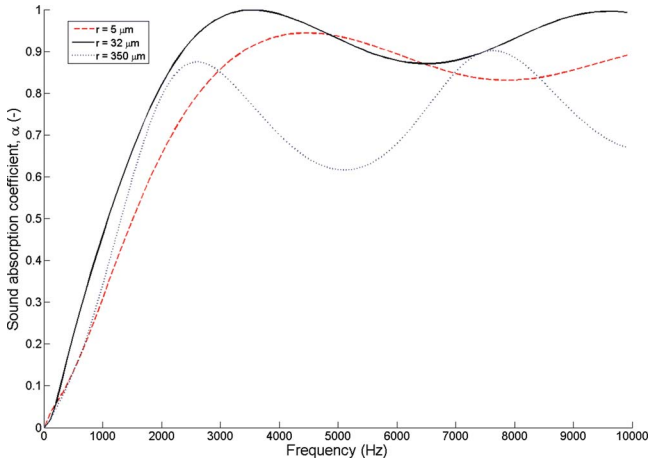

FIG. 4. (Color online) Effect of the fiber radius r in the range 5–350 μm on the sound absorption coefficient. w is fixed at the optimal throat size obtained for $r = 200\ \mu$m, that is, $w = 70\ \mu$m.

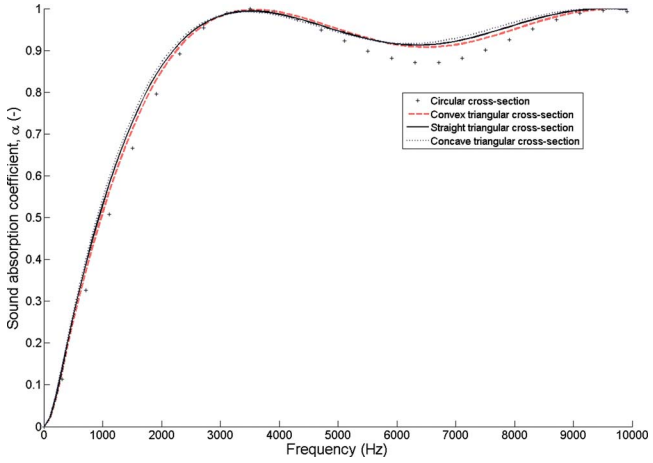

FIG. 5. (Color online) Cross-section shape modification and its effect on the sound absorption coefficient. Triangular cross-section shapes are inscribed in an initial fiber of circular cross-section shape with $r = 32\ \mu$m and $w = 70\ \mu$m.

TABLE III. Numerical evaluation of the main macroscopic parameters associated with a hexagonal porous structure of solid fibers at constant fiber radius $r=32$ μm and thermal characteristic length Λ' for varying inscribed cross-section shapes, i.e., (1) circle, (2) convex, (3) straight, and (4) concave triangle.

Cross-section shape c	Porosity ϕ (%)	Thermal characteristic length length Λ' (μm)	Viscous characteristic length Λ (μm)	Static airflow resistivity σ (N m^{-4} s)	Tortuosity σ_∞ (−)	Performance index I (%)
1	86.21	200	113	26 837	1.07	82.84
2	90.85	201	97	32 661	1.06	84.91
3	92.59	200	82	34 307	1.06	85.39
4	94.56	199	72	35 104	1.06	85.76

firms the potential of Λ minimization as a new sound absorption optimization criterion at constant throat size.

D. Multivariable analysis

The previous analyses focused on specific local geometry parameters and how they individually influence sound absorption. While these analyses provide physical insight, they are not completely rigorous in the sense of a multivariable problem. The relatively small number of calculations performed above does not guarantee that the global optimum has been found in the 3D space of the local parameters (w, r, and c). As commonly used in multivariable optimization problems, the variables identified as having a preeminent role (w and r) on the targeted property (I) can be varied simultaneously to develop a response surface. For example, an identified throat size optimum at constant fiber radius could be different for another different fiber radius. Such a multivariable approach is well appropriate to track the actual optimal (w,r) couples. It also enables extracting practical charts indicating a manufacturer with the aimed fiber radius considering a given controlled throat size, or reciprocally, in order to optimize the produced sound absorber. Furthermore, the global maximum $(w,r)_{\text{opt}}$ is undoubtedly identified, providing an absolute target, with the admissible intervals of variation to stay within 95% of I_{opt}.

A multivariable optimization was performed for different values of w and r in the range $w=[20,200]$ μm and $r=[1,200]$ μm, with c being assigned to circular and triangular cross-section shapes. The results are shown in Fig. 6. For both cross-section shapes, the resulting response surfaces shown by Fig. 6 (top) seem to demonstrate the existence of global maximums. For the case of the circular cross-section shape, $I_{\text{opt}}=85.47\%$ at $(w,r)_{\text{opt}}=(48,6)$ μm. For the case of the triangular cross-section shape, $I_{\text{opt}}=85.91\%$ at $(w,r)_{\text{opt}}=(48,13)$ μm. Furthermore, it appears clearly in Fig. 6 (bottom) that, contrary to the triangular cross-section case for which the optimal throat size is constant for varying radius (straight dotted line), the circular cross-section case shows a more complex relation between optimal throat size and radius (curved dotted line). This different behavior might be interpreted geometrically as follows. Given two triangular cross sections, a fiber radius increase does not significantly modify the solid surface seen by the acoustic wave in the vicinity of the throat. On the contrary, for circular cross sections, a fiber radius increase is associated with a non-neglectable solid surface increase, which is seen by the acoustic wave in the vicinity of the throat, except if the throat size is also increased. Finally, it is of practical interest to mention that, if the fabrication process is advanced enough to produce a fiber pattern keeping the optimal throat size, a relative large tolerance (5–150 μm) is acceptable in terms of fiber radius to stay with 95% of I_{opt}.

E. Comparison with experimental data

Finally, it would be interesting, however not necessary, to compare the results of this bottom-up approach to experimental data. The melamine foam is known to be one of the best acoustic materials in terms of sound absorption. It is often used to design anechoic chambers, and in aeronautic applications. It possesses a highly porous open-cell structure, with very elongated thin ligaments. In some extent, it could be seen as a fibrous structure such as the one described in Fig. 1. The cross-section shape of a melamine foam ligament is made of concave triangles. A scanning electron micrograph of a real melamine foam sample is presented in Fig. 7. A rough estimate of the local geometry parameters can be obtained from such micrographies, yielding $b \simeq 4.3 \pm 0.3$ μm and $l \simeq 46.5 \pm 31.3$ μm (the average length of a ligament on a micrograph is taken as the average length between two ligaments in the model geometry) and $r \simeq 2.5 \pm 0.2$ μm and $w \simeq 41.5 \pm 31.7$ μm. By reporting this couple of local geometry values in the chart of Fig. 6, one can see that this local geometry configuration lies in the best absorption region.

F. Limitations and future works

For practical trend exploration of sound absorption due to porous media morphology, simplifications were made and refined analytical models were not used. However, in the limiting case of fiber radius tending to 0, porosity tends to 1 (i.e., very small fibers concentration), which means that the dimensionless shape factors must tend to zero and that the validity of the results obtained with the Johnson–Allard–Champoux model become questionable. For this reason, a computational check of I was carried out using the refined analytical models in the optimal geometric configuration associated with fibers of circular cross-section shape. The differences for I between Johnson–Allard–Champoux and the refined models were found to be less than 3% (refined mod-

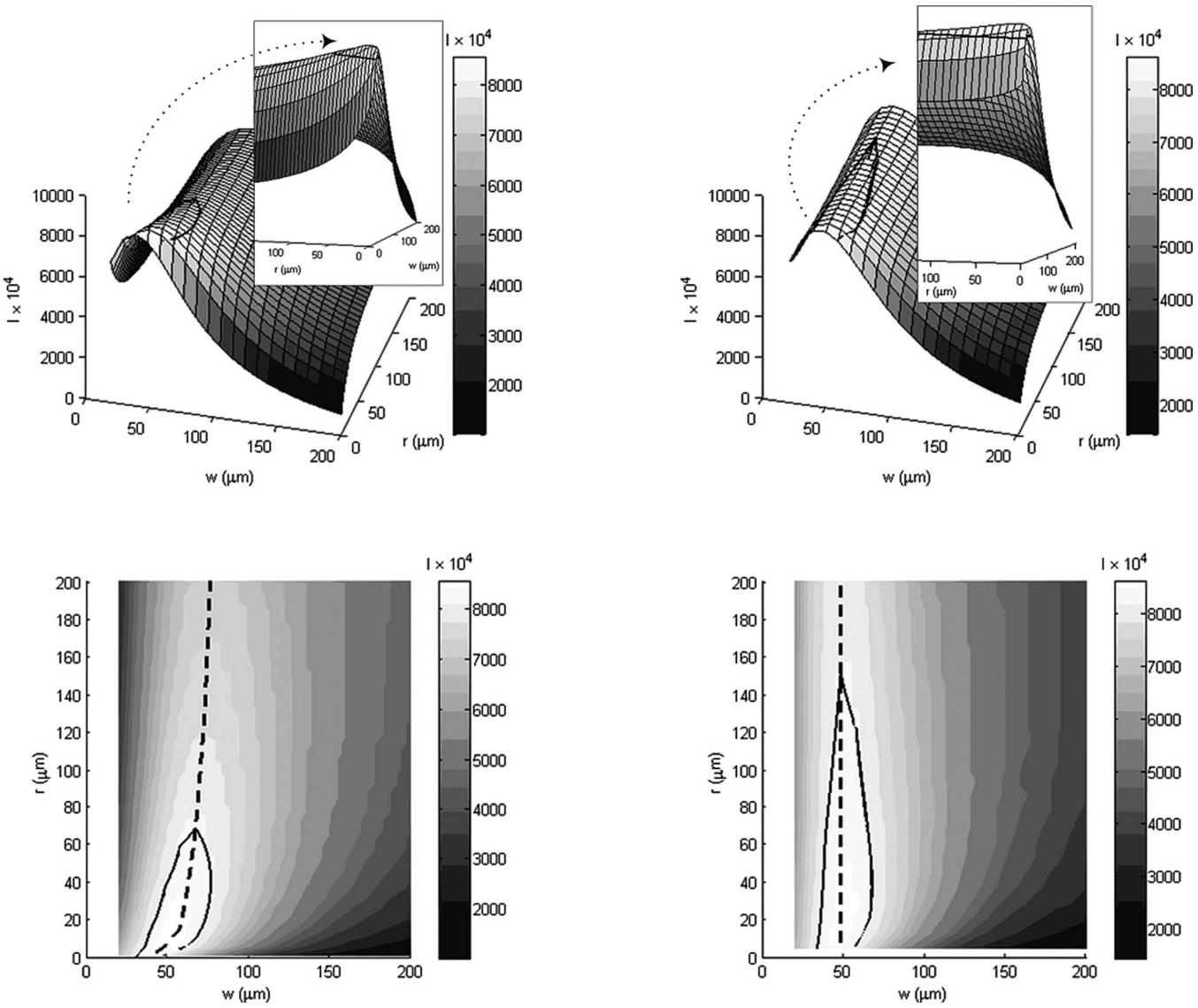

FIG. 6. Response surfaces (top) for the circular (left) and triangular (right) cross-section shape cases and associated 2D map (bottom). Straight lines delimit the $95\% \times I_{\text{opt}}$ zone, and the dotted lines are associated with the optimal (w, r) couples.

els predict better sound absorption performances—notably in the low frequency range). Future works should include (i) a weighting of the low frequency range in the computation of a sound absorption performance index, as well as (ii) a close examination of the acoustical macrobehavior in the limit of small radius using refined models. In particular, the notion of an optimum radius appearing while using the Johnson–Allard–Champoux model needs to be checked. This would also require significant modifications of the fluid-solid boundary conditions.

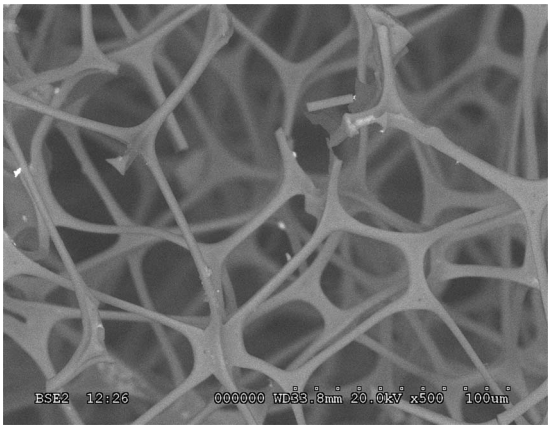

FIG. 7. Scanning electron micrograph of a real efficient sound absorbing melamine foam sample.

IV. CONCLUDING REMARKS

The results of our bottom-up approach for microstructure optimization of sound absorbing materials are summarized in this section. For a given fiber radius, an optimal throat size controlling the sound absorption level can be found, corresponding to an intermediate static airflow resistivity. By contrast, given an optimal throat size, the fiber radius (i.e., cell size) essentially modulates the absorption curve. It is worth mentioning that the optimal absorption curve is the one which minimizes the viscous characteristic length at constant throat size. This property can be used as a

design guide for sound absorption optimization. Another observation is the fact that for a given thermal characteristic length, as the porosity increases from its circular cross-section value to its concave triangular cross section value, the throat size reduces with the viscous characteristic length, enhancing only slightly the sound absorption coefficient of the porous structure but increasing notably its porosity (i.e., reduction of bulk density or weight). Finally, practical investigation charts have been proposed to indicate local geometry parameters tending to maximize the sound absorption coefficient. The validity of these charts was corroborated by comparison with the measured local geometry parameters of a real efficient sound absorbing melamine foam. This confirms the potential of such a bottom-up approach for microstructure optimization of sound absorbing materials.

ACKNOWLEDGMENTS

This work was supported in part by Grants-in-Aid from Alcan, CQRDA, NSERC, and Auto21. A part of the research presented in this paper was also financed by the Fonds Québécois de la Recherche sur la Nature et les Technologies by the intermediary of the Aluminium Research Centre-REGAL. Irène Kelsey from the Material Characterization Center under control of the Materials and Intelligent Systems Institute is gratefully acknowledged for providing technical assistance with scanning electron microscopy.

[1]A. Cummings and S. P. Beadle, "Acoustic properties of reticulated plastic foams," J. Sound Vib. **175**, 115–133 (1994).
[2]R. T. Muehleisen, C. W. Beamer, and B. D. Tinianov, "Measurements and empirical model of the acoustic properties of reticulated vitreous carbon," J. Acoust. Soc. Am. **117**, 536–544 (2005).
[3]R. J. S. Brown, "Connection between formation factor for electrical-resistivity and fluid-solid coupling factor in Biot equations for acoustic waves in fluid-filled porous media," Geophysics **45**, 1269–1275 (1980).
[4]D. L. Johnson, J. Koplik, and R. Dashen, "Theory of dynamic permeability and tortuosity in fluid-saturated porous media," J. Fluid Mech. **176**, 379–402 (1987).
[5]Y. Champoux and J. F. Allard, "Dynamic tortuosity and bulk modulus in air-saturated porous media," J. Appl. Phys. **70**, 1975–1979 (1991).
[6]J. F. Allard, "Modelling sound absorbing materials: Propagation of Sound in Porous Media," edited by Elsevier Applied Science (Elsevier Science, New York, 1993).
[7]S. R. Pride, F. D. Morgan, and A. F. Gangi, "Drag forces of porous media acoustics," Phys. Rev. B **47**, 4964–4975 (1993).
[8]D. Lafarge, P. Lemarinier, J. F. Allard, and V. Tarnow, "Dynamic compressibility of air in porous structures at audible frequencies," J. Acoust. Soc. Am. **102**, 1995–2006 (1997).
[9]A. Craggs and J. G. Hildebrandt, "Effective densities and resistivities for acoustic propagation in narrow tubes," J. Sound Vib. **92**, 321–331 (1984).
[10]X. Wang and T. J. Lu, "Optimized acoustic properties of cellular solids," J. Acoust. Soc. Am. **106**, 756–765 (1999).
[11]M. Y. Zhou and P. Sheng, "First-principles calculations of dynamic permeability in porous media," Phys. Rev. B **39**, 12027–12039 (1989).
[12]M. Firdaouss, J.-L. Guermond, and D. Lafarge, "Some remarks on the acoustic parameters of sharp-edged porous media," Int. J. Eng. Sci. **36**, 1035–1046 (1998).
[13]A. Cortis, D. M. L. Smeulders, D. Lafarge, M. Firdaouss, and J.-L. Guermond, in *IUTAM Symposium on Theoretical and Numerical Methods in Continuum Mechanics of Porous Materials. Series: Solid Mechanics and Its Applications*, University of stuttgart, Germany, edited by W. Ehlers (Kluwer, Dordrecht, 1999), pp. 187–192.
[14]A. Cortis, D. M. J. Smeulders, J.-L. Guermond, and D. Lafarge, "Influence of pore roughness on high-frequency permeability," Phys. Fluids **15**, 1766–1775 (2003).
[15]S. Gasser, F. Paun, and Y. Brechet, "Absorptive properties of rigid porous media: Application to face centered cubic sphere packing," J. Acoust. Soc. Am. **117**, 2090–2099 (2005).
[16]C. Perrot, F. Chevillotte, and R. Panneton, "Dynamic viscous permeability of an open-cell aluminum foam: Computations vs experiments," J. Appl. Phys. **103**, 024909 (2008).
[17]K. Schladitz, S. Peters, D. Reinel-Bitzer, A. Wiegmann, and J. Ohser, "Design of acoustic trim based on geometric modeling and flow simulation for non-woven," Comput. Mater. Sci. **38**, 56–66 (2006).
[18]F. P. Mechel, "Ausweitung der absorberformel von Delany and Bazley zu tiefen frequenzen," Acustica **35**, 210–213 (1976).
[19]D. Lafarge, in *Poromechanics II: Proceedings of the Second Biot Conference on Poromechanics*, edited by J.-L. Auriault (Swets & Zeitlinger, Grenoble, 2002), pp. 703–708.
[20]S. Torquato, "Efficient simulation technique to compute properties of heterogeneous media," Appl. Phys. Lett. **55**, 1847–1849 (1989).
[21]D. A. Coker and S. Torquato, "Simulation of diffusion and trapping in digitized heterogeneous media," J. Appl. Phys. **77**, 955–964 (1994).
[22]C. Perrot, R. Panneton, and X. Olny, "Periodic unit cell reconstruction of porous media: Application to an open cell aluminum foam," J. Appl. Phys. **101**, 113538 (2007).
[23]C. Perrot, R. Panneton, and X. Olny, "Computation of the dynamic thermal dissipation properties of porous media by Brownian motion simulation: Application to an open-cell aluminum foam," J. Appl. Phys. **102**, 074917 (2007).
[24]A. Bhattacharya, V. V. Calmidi, and R. L. Mahajan, "Thermophysical properties of high porosity metal foams," Int. J. Heat Mass Transfer **45**, 1017 (2002).
[25]COMSOL 3.4, WTC-5 pl. Robert Schuman, Grenoble, France.
[26]S. Torquato, "Relationship between permeability and diffusion-controlled trapping constant of porous media," Phys. Rev. Lett. **64**, 2644 (1990), makes implicitly reference to a generalization in harmonic regime of the proof given by Torquato for the symmetry property in static regime.
[27]D. Lafarge, "Propagation du son dans les matériaux poreux à structure rigide saturés par un fluide viscothermique (Sound propagation in rigid porous media saturated by a viscothermal fluid)," Ph.D. thesis, Université du Maine, 1993.
[28]D. Lafarge, "Modèles linéaires de propagation," in *Milieux Poreux et Poreux Stratifiés (Linear models of propagation in Porous Media and Stratified Porous*, Matériaux et Acoustique (Materials and Acoustics), Vol. **1**, edited by M. Bruneau and C. Potel (Lavoisier, Paris, 2006), pp. 143–188.